Dielectric and piezoelectric properties of porous lead-free $0.5Ba(Ca_{0.8}Zr_{0.2})O_3$-$0.5(Ba_{0.7}Ca_{0.3})TiO_3$ ceramics

Yan Zhang, Mengying Xie*, James Roscow, Chris Bowen
Department of Mechanical Engineering, University of Bath, BA2 7AY, UK

Abstract:

Porous barium calcium zirconate titanate $0.5Ba(Ca_{0.8}Zr_{0.2})O_3$-$0.5(Ba_{0.7}Ca_{0.3})TiO_3$ (BCZT) lead-free ferroelectric ceramics were fabricated via a burnt polymer spheres (BURPS) technique by introducing corn starch as the pore-forming agent. The effect of porosity on the microstructure, dielectric, and piezoelectric properties of the porous materials were investigated. An increase in porosity from 10 % to 25 % resulted in an increase in the hydrostatic charge coefficient (d_h), which was 140 to 560 % higher than that of the dense BCZT material. An increase in porosity from 10 % to 25 % also lead to a decrease in relative permittivity that was 16.7% to 60.4% lower than the dense material. These two changes in properties provided a significant enhancement of the hydrostatic figure of merit ($d_h \cdot g_h$) for the porous ceramic; for example the $d_h \cdot g_h$ of the 25 vol.% porous BCZT ceramic was 158 times more than the dense ceramic and demonstrates the potential of porous lead-free ferroelectrics for piezoelectric transducer devices. Reasons for the significant enhancement in piezoelectric performance of the porous ceramics are discussed.

Highlights:

- ✓ Porous lead-free piezo-ceramics were fabricated by introducing pore-forming agents.
- ✓ An increase in porosity increased hydrostatic charge coefficient and decreased permittivity.
- ✓ Hydrostatic parameters g_h and $d_h \cdot g_h$ of the porous ceramic were 140% to 560% higher than the dense material.

Introduction

$Pb(Zr,Ti)O_3$-based (PZT) piezoelectric ceramics are commonly utilized in a variety of sensors, actuators, and ultrasonic transducers. Due to legislation that aims to restrict the use of lead based products and environmental concerns regarding the toxicity of lead/lead oxide and its recycling and disposal when used during the production process, there is an increasing demand for replacing it with lead-free alternatives. Amongst the variety of lead-free materials, barium calcium zirconate titanate whose chemical formula is $0.5Ba(Ca_{0.8}Zr_{0.2})O_3$-$0.5(Ba_{0.7}Ca_{0.3})TiO_3$ (hereafter abbreviated as BCZT) is one of the most widely studied lead-free piezoelectric ceramic [1-3]. The material is of interest since its piezoelectric properties are comparable, and even superior, to other lead free compounds such as the conventionally used lead-based piezoelectric ceramics in terms of the 'hard' and 'soft' PZTs, PMN-PT (lead magnesium niobate-lead titanate) and PZN-PT (lead zinc niobate-lead titanate). The piezoelectric coefficient (d_{33}) of the BZCT ceramic with the stoichiometric ratio highlighted above was reported to be in the range of 550-640 pC/N[4]; which was almost the highest values to-date for lead-free materials. This promising result has attracted increasing scientific interest of the employment of this lead-free ceramics in transducer applications and replacing current lead-based ferroelectrics.

To date, the majority of the literature has focused on tailoring the properties of *dense* BCZT by doping[5, 6], texturing[7, 8] and optimising the processing conditions[9, 10] to increase its Curie temperature (T_c) or further improving its piezoelectric performance in terms of piezoelectric

coefficient and permittivity. An effective way to assess the performance and properties of ferroelectric materials for practical piezoelectric and pyroelectric applications is to compare appropriate *figures of merit (FoM)* which contain combinations of relevant physical properties. These *FoMs* have been utilised widely for assessment of materials for a range of applications, for example $\frac{d_{ij}^2}{\varepsilon_r \varepsilon_0}$ for piezoelectric energy harvesting, $\frac{p^2}{\varepsilon_r \varepsilon_0 \times (C_E)^2}$ for pyroelectric energy harvesting, and $\frac{(d_{33}+2d_{31})^2}{\varepsilon_r \varepsilon_0}$ for hydrostatic and SONAR applications, where d_{ij} is the piezoelectric charge coefficient, ε_r is the relative permittivity (or dielectric constant), ε_0 is the permittivity of free space, p is the pyroelectric coefficient, d_{33} and d_{31} are the longitudinal and transverse piezoelectric charge coefficients respectively. We can see in the above *FoMs* that the permittivity of the material is included in all of the equations and is inversely proportional to each *FoM*; this indicates that a lower permittivity is beneficial to achieve a high performance if the piezoelectric and pyroelectric coefficient remains unchanged. However, the relative permittivity of ferroelectrics is typically very high; for example for dense BCZT, ε_r > 2100 at room temperature. One approach to achieve a high *FoM* is to introduce low permittivity pores into the dense material [11, 12]. Therefore a detailed understanding of effects of porosity on ferroelectric and piezoelectric properties in such piezoelectric lead-free material systems is beneficial in understanding how to enhance and tailor the desired properties of these new materials.

This paper provides the first experimental measurements on porous BCZT ceramics to understand the effect of porosity on ferroelectric and piezoelectric properties of these lead-free ferroelectrics. The objective of this work is to analyse the microstructure, dielectric, and piezoelectric properties of porous BCZT ferroelectric ceramics that have been manufactured using volatile additions that burn out during the high temperature sintering process, known as the 'BURPS technique'. The properties will be correlated with porosity, and the underlying physical mechanisms for the observed changes in properties will also be explained.

Experimental

BCZT powders and porous BCZT ceramics were prepared by a solid-state reaction approach and the BURPS technique (Burnt Polymer Spheres). Analytical grade (Sigma Aldrich) $BaCO_3$ (99%), $CaCO_3$ (99%), TiO_2 (99.9%), and ZrO_2 (99%) were selected as starting materials and weighted according to the stoichiometric ratio. After 4h of ball-milling, the mixtures were calcined at 1200 °C for 3 h and followed by additional ball-milling for 24 h. The milled powders were mixed for 12h with ethanol and different additions of the pore forming agent, corn starch powder (0, 5, 16, 25, 34, 48 wt.% based on the calcined powders), followed by mixing with the 1 wt.% PVA binder for both dense and porous samples. After drying, the powders were uni-axially cold-compacted to form pellets of 13 mm in diameter and 1.5mmin in thickness. The cold-compacted pellets were first heated to 600 °C for 3h to remove the organic additives and then sintered at 1400 °C for 4 h to achieve the final samples.

The phase structure of the ceramics was examined by X-ray diffractometer (BRUKER D8-Advance, USA) with Cu radiation with 2θ ranging from 20°-70°. The microstructure of the sintered samples was investigated by a scanning electron microscopy (SEM, JSM6480LV, Tokyo, Japan). The bulk density of the sintered specimens was measured using the Archimedes' principle. For evaluation of the electrical properties, silver paint was coated on both faces of the sintered samples to form electrodes. For piezoelectric measurements, the ceramics were electrically poled using the corona poling by applying a DC voltage of 14 kV for 30 min at 60 °C. Maximum polarization, remnant polarization and coercive field, were measured using a Radiant RT66B-HVi Ferroelectric Test system on initially unpoled materials. The temperature and frequency dependence of the dielectric constant was studied using an impedance analyzer (Solartron 1260, Hampshire, UK) in a temperature and frequency range of 30-150 °C and 1-10^5 Hz. The longitudinal piezoelectric strain coefficient (d_{33}) and the transverse piezoelectric strain coefficient (d_{31}) were measured using a Berlincourt Piezometer (PM25, Take Control, UK).

Results and discussions

Figure 1(A) and (B) show the X-ray diffraction pattern and scanning electron microscopy (SEM) image of the as-synthesized BCZT powder, respectively. As seen in Figure 1(A), strong XRD peaks with a small full width at half maximum (FWHM) values were observed which indicates that the synthesized powders were well crystallized. No trace of the presence of secondary phases was found in the diffractogram, neither reflection splitting nor super-lattice reflections were observed. The XRD patterns of $BaTiO_3$-based BCZT phase showed good agreement with the conventional tetragonal $BaTiO_3$ structure with the P4mm space group from the JCPDS card number 05-0626. Intense diffracted peaks observed at 2θ = 22.27°, 31.63°, 39°, 44.91°, 45.36°, 51.02°, 56.38° that correspond to the *(hkl)* Miller index of (100), (110), (111), (002), (200), (210), (211) planes respectively. The electrostatic Coulomb repulsions between 3d electrons of Ti^{4+}/Zr^{4+} ions and 2p electrons of O^{2-} ions led to the distorted crystal structure in the $BaTiO_3$-based ceramic, resulting in a stable tetragonal structure. The splitting of the (200) peak of the pure BCZT into (002) and (200) peaks in the 2θ range of 44°-46° at room temperature corresponding to Ca^{2+} (A-site) and Zr^{4+} (B-site) ions diffusing into Ba^{2+} (A-site) and Ti^{4+} (B-site), respectively confirmed the tetragonal or tetragonal-dominant phase formation[13]. The BCZT powders after ball milling exhibited an irregular shape with an average size of approximately 1 µm, as can be seen in Figure 1(B).

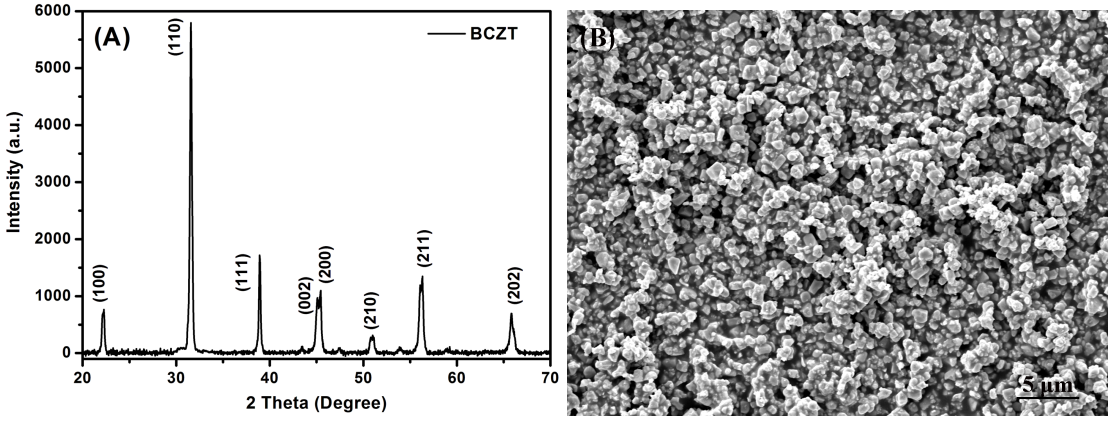

Figure 1 (A) XRD spectrum and (B) SEM micrograph of BCZT powders after ball milling.

Figure 2 (A) and (B-F) show SEM images of the cross-sections of the dense and porous BCZT with a porosity range of 10 % to 25 %, which correspond to corn starch additions from 5 wt.% to 48 wt.%. As can be seen in Figure 2, a microstructure with a fully densified polycrystalline matrix and struts can be clearly seen for all the materials which were sintered at 1400 °C; this indicates that the BCZT powders were well sintered under this processing condition. From Figure 2(A), the dense BCZT ceramic, which had no pore forming agent added, was highly dense with a measured porosity of approximately 4 %. As the amount of pore-former (corn starch) was increased from 5 wt.% to 48 wt.%., the number of the pores in the microstructure increased, which can be seen in Figures 2(B-F). Large pores are likely to be generated by the coalescence of pores and there is likely to be an increase in the interconnection of pores as the amount of pore former increased, e.g. the pore size increased to approximately 20 µm when the porosity volume fraction was 25 %, compared with the pore size of 5 µm for the material with only 10 % porosity. The microstructures for all levels of porosity exhibited homogeneously distributed pores, with spherical and mostly open pores in the matrix. This was attributed to the shape of the corn starch pore-former, because pore formed as a result of decomposition of the organic phases. It was also seen that a continuous porous network was formed in the porous BCZT ceramics and the homogeneous pore distribution led to the formation of a strong pore wall network.

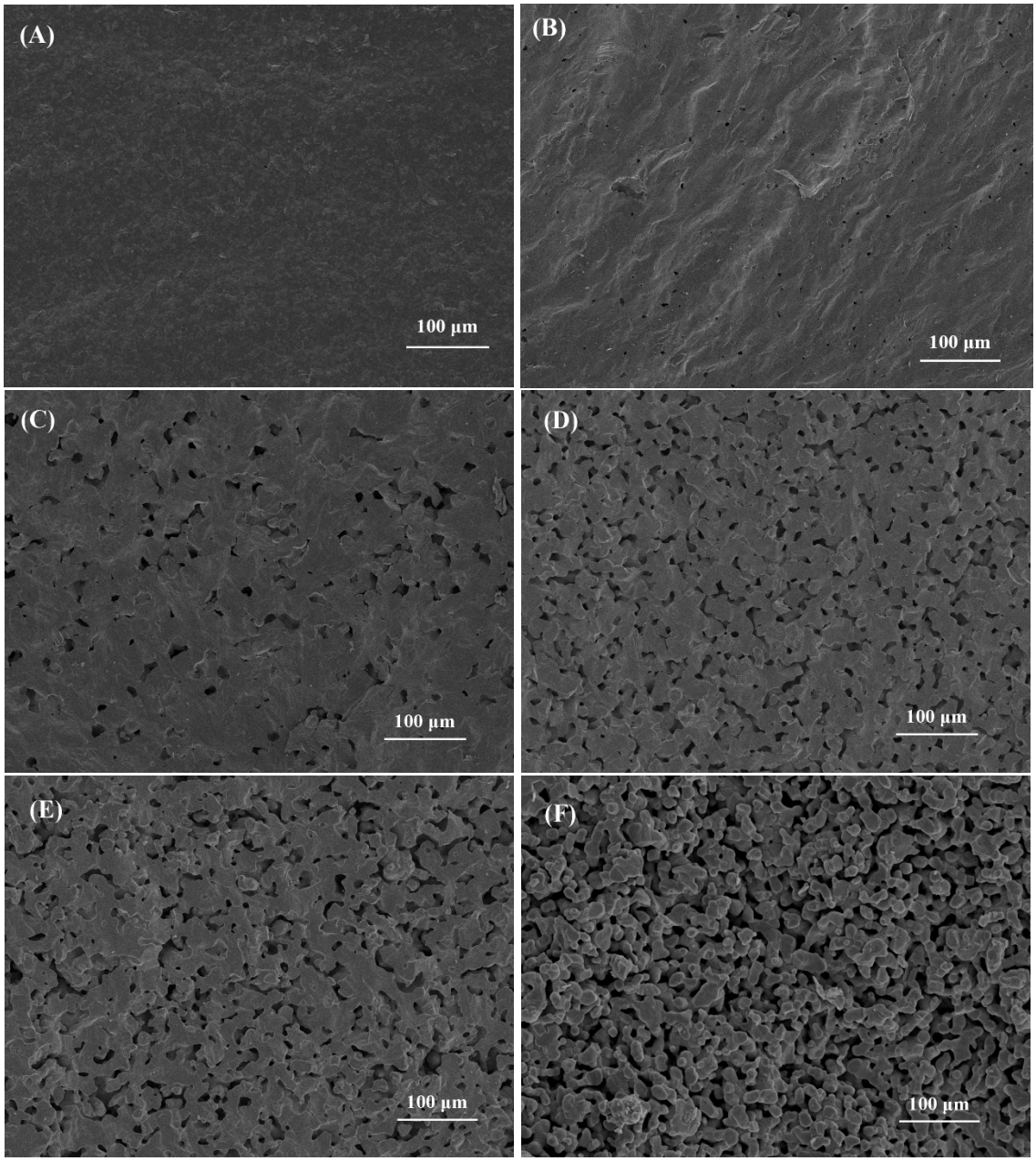

Figure 2 SEM micrographs of (A) dense and porous BCZT ceramics with the porosity fractions of (B) 10 %, (C) 15 %, (D) 18 %, (E) 21 %, (F) 25 %.

Figure 3 shows the polarisation-field (P-E) loop of the dense and porous BCZT ceramics with different porosity levels at ambient temperature. The porous materials exhibited both a lower remnant polarisation (P_r) and coercive electric field (E_c) compared to the dense BCZT ceramic; which were 7.69 µC/cm^2 and 2.62 kV/cm, respectively for the dense material. The hysteresis loops of the porous materials exhibited a symmetrical shape, indicating a good ferroelectric response for all the BCZT materials. Both the P_r and E_c can be influenced by the porosity, as the presence of the pores can change the domain movement under electric field. Figure 3 shows that as the porosity increased from 10 % to 25 % the P_r decreased from 5.86 µC/cm^2 to 3.84 µC/cm^2, while the E_c gradually decreased from 1.77 kV/cm to 1.51 kV/cm. The presence of the passive pore phase (air) in the porous BCZT resulted in a reduced fraction of the active BCZT ferroelectric ceramics per unit volume which led to the decreased remnant polarisation. The decrease of the coercive field as the porosity increased from 10 to 25 % is

likely due to the reduced internal stress in the vicinity of the pores and higher compliance of the porous matrix which facilitates the ease of domain switching.

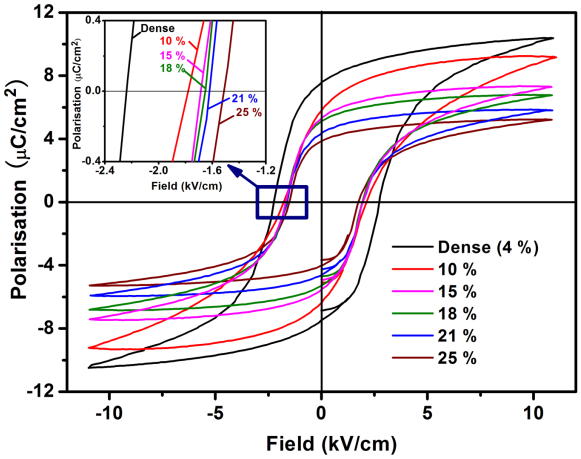

Figure 3 Ferroelectric hysteresis loops of dense and porous BCZT with different porosities.

Figure 4 shows the relative permittivity and dielectric loss of the dense and porous BCZT ceramics at a range of frequencies and temperatures. The frequency dependence of the relative permittivity and dielectric loss of BCZT were measured at room temperature for the different porosity levels, and are presented in Figure 4 (A) and (B). All the porous ceramics exhibited a lower relative permittivity and higher dielectric loss than that of the dense BCZT. For instance, the relative permittivity at 1 kHz of the porous BCZT reduced from 2158 to 1026 when the porosity fraction increased from 10 % to 25 %, which was 16.7 % to 60.4 % lower than that of the dense BCZT at room temperature (ε_r = 2590). It can be seen that in the low frequency range (≤ 500 Hz) the dielectric loss of both the dense and porous BCZTs increases with decreasing frequency and the behaviour of the material in this low frequency range is associated with a small level of dc conductivity in the material; i.e. a conduction loss [14]. After a minimum loss at ~1 kHz the loss then begins to increase with increasing frequency above ~2 kHz. This high frequency loss is likely to be associated with the onset of ionic relaxation losses.
Figure 4(C) and (D) show the temperature dependence of the relative permittivity and dielectric loss. The peak of permittivity curve, or the turning point of the tangent loss curves, correspond to the Curie temperature (T_C) of the ferroelectric ceramic, where dense BCZT exhibited a T_C of approximately 106 °C. When the temperature was lower than T_C, the increase in permittivity with temperature can be accredited to an increase in the conductivity of both the dense and porous BCZTs, and therefore an increased permittivity and dielectric loss was achieved. When the temperature (T) was higher than T_C, the relative permittivity of all BCZT ceramics reduced according to the Curie-Weiss law ($\varepsilon_r=C/(T-T_C)$, and C *i*s the Curie-Weiss constant) and is widely used to describe the change of the permittivity. The dielectric loss of the porous BCZT materials followed a similar trend with equally low values as the dense BCZT at different frequencies and temperatures and this was attractive in terms of reducing the energy loss from the ferroelectric composite (BCZT/air). Moreover, one can see that the T_C of the porous BCZT slightly increased from 107-111 °C as the porosity level increased, this was attributed to the stress relaxation near the pore area, similar to that of our porous PZT materials with the porosity from 25 to 45 %[12]. This suggested that the porosity ranging from 10 to 25 % imposed small effects on the phase transition and change of the crystalline structure of the porous BCZT ceramics when employing corn starch as the pore forming agent.

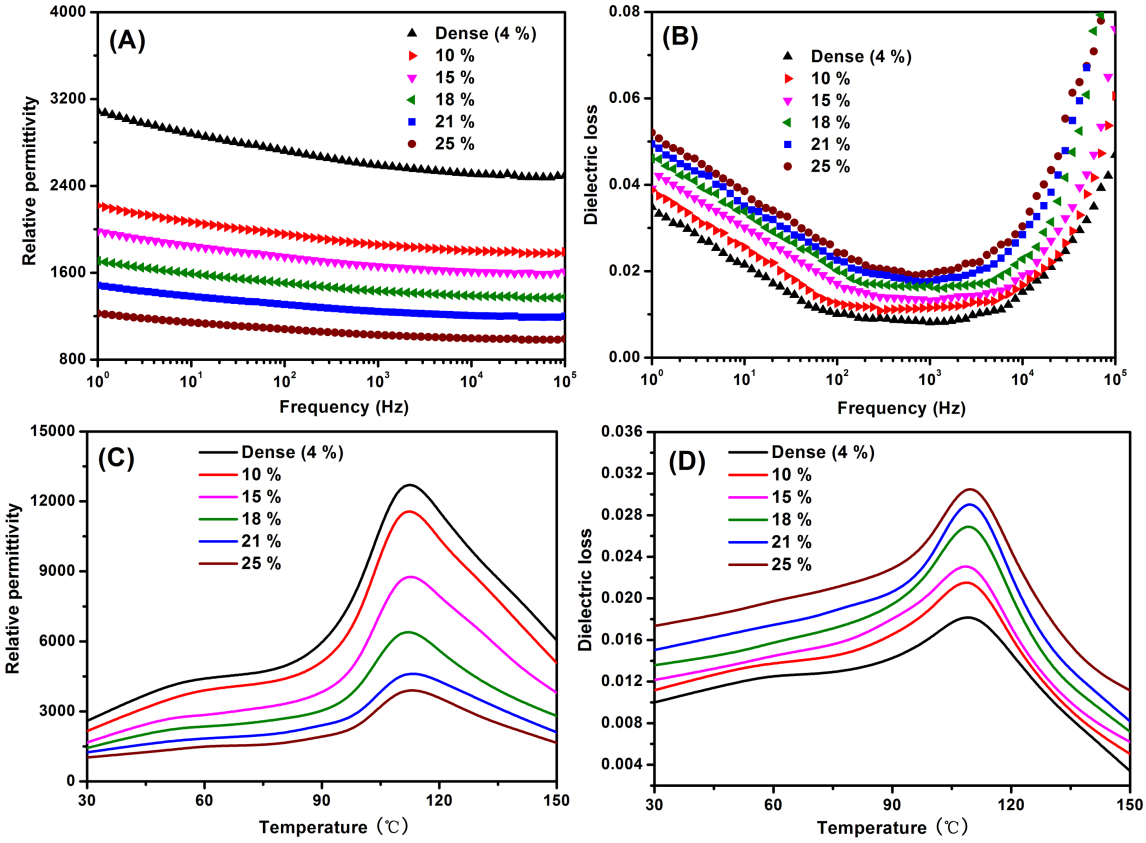

Figure 4 Relative permittivity and dielectric loss of porous BCZT with different (A) (B) frequencies at room temperature and (C) (D) temperatures at 1 KHz frequency.

Figure 5(A) and (B) show the variation of the piezoelectric coefficients and hydrostatic parameters of the BCZT ceramics with porosity level. It can be seen from the Figure 5(A) that the longitudinal (d_{33}) and transverse (d_{31}) piezoelectric coefficients decreased as the porosity fraction increased. However, the hydrostatic charge coefficient (d_h) increased as the porosity level in the BCZT materials increased. Specifically, the d_{33} and d_{31} values of the porous BCZT decreased from 424 to 285 pC/N and -195 to -96 pC/N while the d_h increased from 34 to 93 pC/N when the porosity increased from 10 to 25%; this corresponded to a 19-46% and 24-62% decrease and 140-560% increase compared the dense ceramic which exhibited a d_{33}, d_{31} and d_h of 524, -255 and 14 pC/N respectively. The decrease in the piezoelectric coefficients (d_{33}, d_{31}) with increasing porosity is related to the reduced fraction of piezoelectric phase per unit volume which leads to a reduced remnant polarisation (Figure 3) and piezoelectric response. Secondly, it is know that during the poling process the electric field concentrates inside the low permittivity pore region, also leading to reduced polarisation, according to our previous modelling results [11]. However the larger decrease in d_{31}, compared to d_{33}, leads to the porous material exhibiting a higher d_h, see Figure 5(A).

It is evident in Figure 5 (B) that the porous BCZT shows a pronounced increase of hydrostatic voltage coefficient ($g_h=d_h/\varepsilon_0\varepsilon_r$) and hydrostatic figure of merit (d_hg_h), where d_h is the hydrostatic charge coefficient ($d_h=d_{33}+2d_{31}$). For the dense BCZT ceramic in this work, d_{33} is almost equivalent $-2d_{31}$ which led to a very low d_h of 14 pC/N, and when combined with its high relative permittivity (ε_r = 2590) this resulted in the dense ceramic exhibiting a low d_h, g_h, and $d_h \cdot g_h$, thereby limiting their performance as a transducer material under hydrostatic conditions. However the introduction of porosity and reduction is d_{31} and permittivity lead to a greatly increased d_h (Figure 5(A)), g_h (Figure 5(B)) and $d_h \cdot g_h$ (Figure 5(B)). It can be seen that g_h and $d_h \cdot g_h$ increased with increasing porosity with the highest value of $g_h \sim 10.2\times10^{12}$ Vm/N and $d_h \cdot g_h \sim 0.95\times10^{12}$ m^2/N, this is approximately 17 and 158 times higher than that of dense BCZT materials ($g_h \sim 0.61\times10^{12}$ Vm/N and $d_h \cdot g_h \sim 0.008\times10^{12}$ m^2/N).

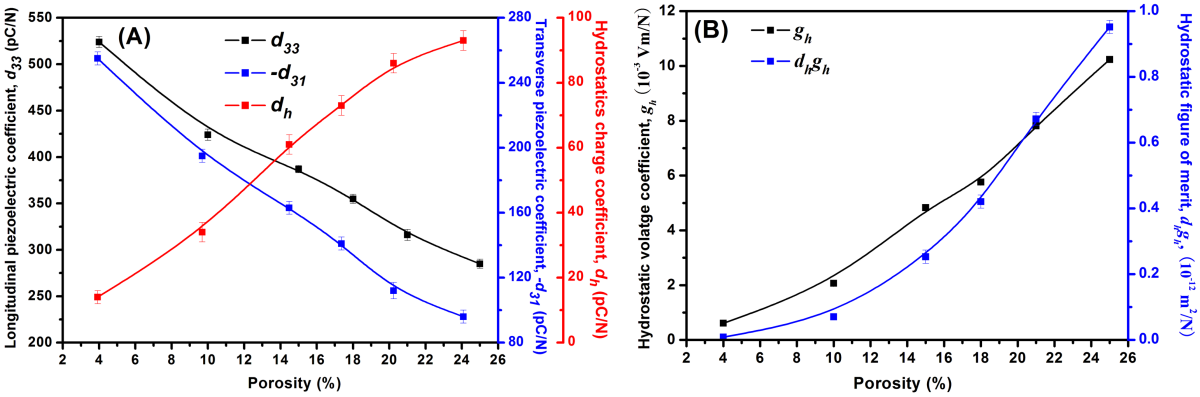

Figure 5 (A) Piezoelectric coefficients and (B) hydrostatic parameters of porous BCZT with the porosity ranging from 10 to 25 %.

Conclusions

Porous $0.5Ba(Ca_{0.8}Zr_{0.2})O_3$-$0.5(Ba_{0.7}Ca_{0.3})TiO_3$ (BCZT) lead-free ceramics were produced by using volatile additives at different additions of the pore forming agent. The microstructure, piezoelectric and dielectric properties of porous PZT–PCN ceramics were investigated in detail as a function of the porosity. The relative permittivity of the porous BCZT decreased from 2158 to 1026, while dense ceramic exhibited a relative permittivity of 2590. There was also a large decrease in the longitudinal piezoelectric coefficient as the porosity content increased. These factors were beneficial to the performance figures of merit for future material election and design for transducer applications. Moreover, the loss tangents of the composites remained relatively low, which was preferred in terms of reducing the energy loss from a dielectric material. Enhanced piezoelectric properties for the lead-free porous $0.5Ba(Ca_{0.8}Zr_{0.2})O_3$-$0.5(Ba_{0.7}Ca_{0.3})TiO_3$ ceramics were demonstrated with a d_h~93 pC/N, g_h~10.237×10^{12} Vm/N and $d_h \cdot g_h$~0.952×10^{12} m^2/N are demonstrated at the maximum level of 25 % porosity. Thus, these porous BCZT with low dielectric loss and high performance are suitable for many practical transducer applications such as piezoelectric sensors and energy harvesters and exhibit competitive sensitivities compared to the lead-based equivalent materials.

Acknowledgement

Dr. Y. Zhang would like to acknowledge the European Commission's Marie Skłodowska-Curie Actions (MSCA), through the Marie Skłodowska-Curie Individual Fellowships (IF-EF) (H2020-MSCA-IF-2015-EF-703950-HEAPPs) under Horizon 2020. Prof. C. R. Bowen, Dr. M. Xie and Mr J. Roscow would like to acknowledge the funding from the European Research Council under the European Union's Seventh Framework Programme (FP/2007–2013)/ERC Grant Agreement no. 320963 on Novel Energy Materials, Engineering Science and Integrated Systems (NEMESIS).

References

[1] X. Chao, J. Wang, Z. Wang, T. Zhang, Z. Yang, G. Li, Materials Research Bulletin, 76 (2016) 450-453.
[2] J. Wu, A. Habibul, X. Cheng, X. Wang, B. Zhang, Materials Research Bulletin, 48 (2013) 4411-4414.
[3] P. Wang, Y. Li, Y. Lu, Journal of the European Ceramic Society, 31 (2011) 2005-2012.
[4] W. Liu, X. Ren, Physical Review Letters, 103 (2009) 257602.
[5] X. Liu, D. Wu, Z. Chen, B. Fang, J. Ding, X. Zhao, H. Luo, Advances in Applied Ceramics, 114 (2015) 436-441.
[6] P. Parjansri, K. Pengpat, G. Rujijanagul, T. Tunkasiri, U. Intatha, S. Eitssayeam, Ferroelectrics, 458 (2014) 91-97.

[7] Z.-H. Zhao, X.-L. Li, Y.-J. Dai, M.-Y. Ye, H.-M. Ji, Ceramics International, 42 (2016) 18756-18763.
[8] Z. Zhao, X. Li, Y. Dai, H. Ji, D. Su, Materials Letters, 165 (2016) 131-134.
[9] W. Li, Z. Xu, R. Chu, P. Fu, G. Zang, Materials Science and Engineering: B, 176 (2011) 65-67.
[10] J. Wu, D. Xiao, W. Wu, J. Zhu, J. Wang, Journal of Alloys and Compounds, 509 (2011) L359-L361.
[11] M.X. Yan Zhang, James Roscow, Yinxiang Bao, Kechao Zhou, Dou Zhang, Chris R. Bowen., Journal of Materials Chemistry A, 5 (2017) 6569-6580.
[12] Y. Zhang, Y. Bao, D. Zhang, C.R. Bowen, Journal of the American Ceramic Society, 98 (2015) 2980-2983.
[13] K. Miura, M. Azuma, H. Funakubo, Materials, 4 (2011) 260.
[14] C.R. Bowen, D.P. Almond, Materials Science and Technology, 22 (2006) 719-724.